The Planetary Science Journal, 3:197 (10pp), 2022 August https://doi.org/10.3847/PSJ/ac82aa

Assessing the Detectability of Europa's Seafloor Topography from Europa Clipper's Gravity Data

Ze-Wen Koh[1], Francis Nimmo[2], Jonathan I. Lunine[1], Erwan Mazarico[3], and Andrew J. Dombard[4]
[1] Department of Astronomy, Cornell University, 122 Sciences Drive, Ithaca NY 14853, USA; zk74@cornell.edu
[2] Department of Earth and Planetary Sciences, University of California Santa Cruz, 1156 High Street, Santa Cruz, CA 95064, USA
[3] Goddard Spaceflight Center, Mail Code 698, Greenbelt, MD 20771, USA
[4] Department of Earth and Environmental Sciences, University of Illinois at Chicago, 845 W. Taylor Street (MC-186), Chicago, IL 60607, USA
Received 2022 May 19; revised 2022 July 17; accepted 2022 July 18; published 2022 August 19

Abstract

Due to its size and tidal heating, Europa may potentially possess active volcanism and hydrothermal circulation at its seafloor. The upcoming Europa Clipper mission provides the opportunity to obtain global gravity maps over a range of spatial scales, up to degree $l \approx 10$. We assess the ability of such gravity measurements to determine Europa's seafloor topography, building on and extending previous work in this area. We create a suite of models that test the gravity signature of a wider range of possible topographies and lithospheric thicknesses, spacecraft close-approach altitudes, and the effect of a gypsum layer on the seafloor. Additionally, we model Europa's seafloor scaled from other geologically active bodies, i.e., Earth, Venus, and Io, investigating the distinguishability of volcanic or plate tectonic features. We find that seafloor topography should be detectable at the resolution of Clipper, while the ice shell characteristics (e.g., via admittance analysis) are not resolvable globally. In our baseline scenario, seafloor topography dominates the total gravity signal up to degree $l = 22$, while for planetary analogs this proves true up to degree $l = 11$ for an Earth-scaled seafloor, as well as $l = 42$ and $l = 54$ for a Venus- or Io-scaled seafloor. Finally, we find that a putative layer of gypsum on the seafloor reduces the gravity signal by flattening out the seafloor, though its presence will not be detectable absent independent determination of its topographic amplitude.

Unified Astronomy Thesaurus concepts: Europa (2189); Galilean satellites (627); Gravitational fields (667)

1. Introduction

Since the Galileo orbiter's discovery of an ocean underneath the ice shell, models of Europa's internal structure have established that the ocean is underlaid by a silicate mantle (Schubert et al. 2009). The topography of the silicate mantle's surface, which we call here Europa's seafloor, could provide indirect evidence for how the lunar-sized silicate body within Europa operates geologically (Dombard & Sessa 2019). Europa's size and tidally heated state imply the potential for active volcanism and hydrothermal circulation at the seafloor, while at the same time thinning the lithosphere. Untangling these effects requires a high-quality gravity map over a range of spatial scales. Determination of the geologic style and state of activity of the silicate mantle's surface is important to understanding whether the ocean is a plausible environment for life (Russell et al. 2010).

The upcoming Europa Clipper mission, planned for launch in the middle of this decade, will be the best opportunity for global-scale, detailed gravity measurements. The mission plan includes several dozen flybys, covering each latitudinal region with altitudes as low as 50 km (Verma 2018). The expected spatial resolution of the recovered gravity field is up to spherical harmonic degree $l \approx 10$ (Mazarico et al. 2021). Although the gravity signal of the seafloor is attenuated owing to the presence of the water layer above, the higher density and mass of the silicate layer causes it to dominate at longer wavelengths (Pauer et al. 2010), providing an opportunity to infer the seafloor topography.

In order to assess the Europa Clipper mission's ability to estimate Europa's seafloor topography from the gravity data it collects, we create a suite of models that explore the possible parameter space that Europa Clipper may observe. We build on and extend previous work in this area (Pauer et al. 2010), including testing of the gravity signature of a wider range of possible topographies and lithospheric thicknesses (Dombard & Sessa 2019), and spacecraft close-approach altitudes. Recent results from Melwani Daswani et al. (2021) also suggest that during Europa's formation warmer temperatures could have led the interior to release volatiles, creating a carbonic ocean. As pressures decrease, gypsum ($CaSO_4$) saturates and precipitates, potentially forming a 3–10 km layer of gypsum on the seafloor. Hence, we also investigate the effect of such a layer of gypsum on the seafloor. Lastly, we consider the possibility of a Europan seafloor modeled after other geologically active terrestrial bodies in our solar system, namely, Earth, Venus, and Io. Through this we explore the distinguishability of features like mid-ocean ridges or shield volcanism, and hence whether Europa Cipper data could deduce their existence under Europa's ocean.

2. Model Approach

Our model includes four contributing sources to the total gravity field observed by Europa Clipper (see Figure 1): (a) the degree-2 shape of Europa caused by tidal and rotational effects, (b) short-wavelength topography at the surface and at the ice–ocean interface, (c) long-wavelength variations in the ice shell thickness, and (d) the seafloor topography. Because here we are

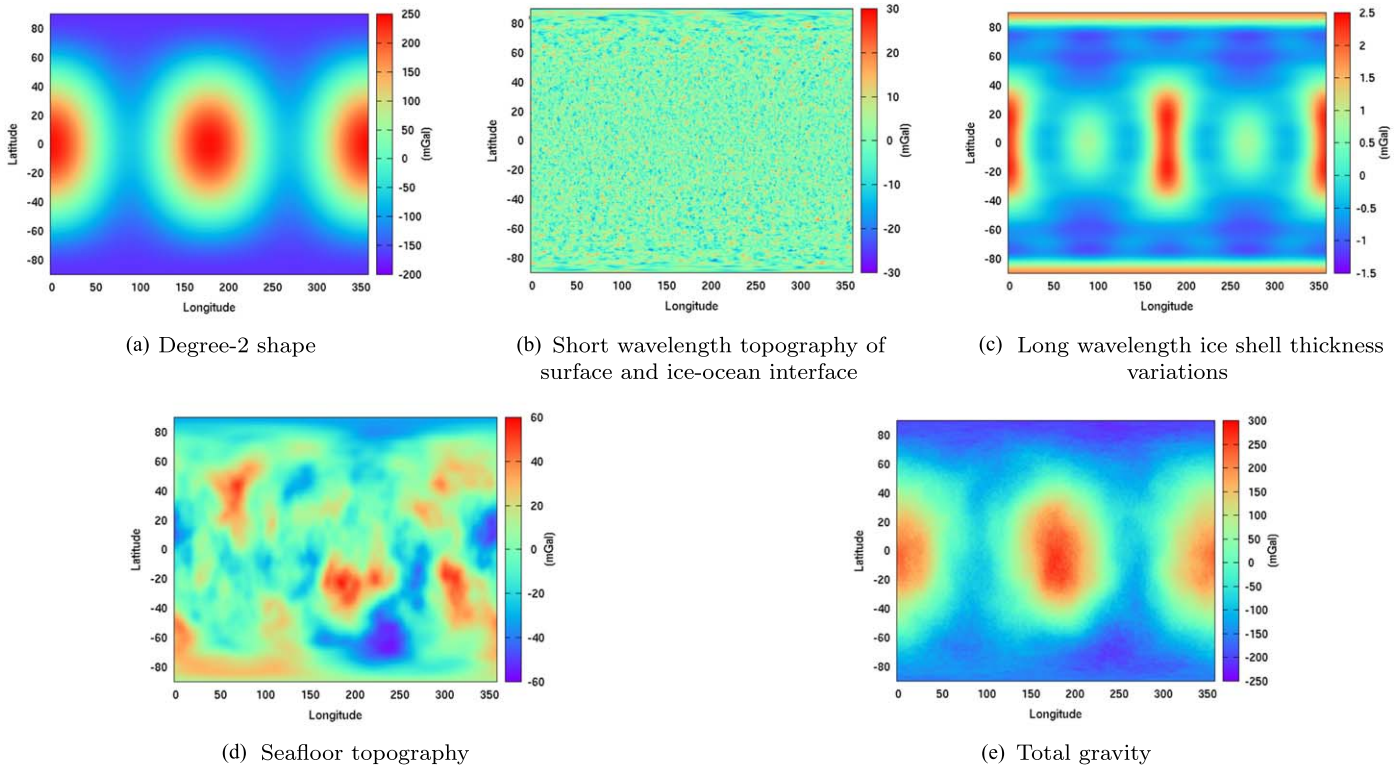

(a) Degree-2 shape

(b) Short wavelength topography of surface and ice-ocean interface

(c) Long wavelength ice shell thickness variations

(d) Seafloor topography

(e) Total gravity

Figure 1. Panels (a)–(d) show the gravity signal in mGal from the four listed sources, of which (d) the seafloor topography is our parameter of interest. Panel (e) shows the total gravity that results from combining the prior four signals.

interested in (d) seafloor topography, we focus on examining how it affects the total gravity signal depending on which parameters are varied. The other three sources are held constant and are based on best estimates from limb profiles obtained by Galileo (Nimmo et al. 2007), described in the Appendix. Figure 1 shows the four contributing sources (a)–(d), as well as the total gravity from summing them.

To study the effect of a range of seafloor topographies, we first generate a random set of spherical harmonic coefficients C_{lm} and S_{lm} of degree l and order m. The randomized topography h at any given point is then expressed as

$$h(\theta, \phi) = R_0 \sum_{l=2}^{N} \sum_{m=0}^{l} \overline{P}_{lm}[\cos(\theta)] \times (\overline{C}_{lm} \cos m\phi + \overline{S}_{lm} \sin m\phi), \quad (1)$$

where θ is the colatitude, ϕ is the longitude, R_0 is the mean radius of Europa (approximated to be 1560.77 km), P_{lm} is an associated Legendre polynomial, and overbars denote normalized coefficients. We use a maximum spherical harmonic degree N of 150, and the $\overline{C}_{lm}$ and $\overline{S}_{lm}$ coefficients are normalized such that

$$C_{lm} = \overline{C}_{lm} \sqrt{(2 - \delta_{0m})(2l + 1)(l - m)!/(l + m)!}\,. \quad (2)$$

These spherical harmonic coefficients are then adjusted initially to follow a power law, known as Kaula's law (see Figure 2(a)). The varying amplitudes and slopes of this power spectrum characterize the range of topographies we explore by determining peak-to-peak difference in global topography and the smoothness of the seafloor, respectively. As our "base" topography, we assume a total estimated amplitude of 2 km and a spectral slope β of -1.8 (Pauer et al. 2010). Figure 2 shows the power spectrum of topography and gravity, respectively, where these default parameters for the topographic power spectrum are assumed.

In order to convert this topography into a corresponding gravity signal, we calculate the gravity coefficients from the topography as follows (Jeffreys 1976):

$$C^g_{lm} = \frac{l + 1}{2l + 1} 4\pi G \Delta\rho \left(1 - \frac{z}{R}\right)^{l+2} C^h_{lm} \quad (3)$$

and equivalently for S_{lm}, where superscripts g and h refer to the gravity and topography coefficients, respectively, $\Delta\rho$ is the density contrast at the interface, and z and R are the radial distances from the interface and center of Europa, respectively, to where the gravity is calculated. Thus, if we are calculating the gravity at the surface due to the mantle topography, z will be the thickness of the hydrosphere and $\Delta\rho$ will be the rock–water density contrast. The gridded gravitational acceleration $g(\theta, \phi)$ is then calculated from the set of spherical harmonic coefficients equivalent to Equation (1). Note that this equation assumes that the topography is uncompensated (see below) and does not take into account finite-amplitude effects at high degrees (Phillips & Wieczorek 1998), though this effect has been shown to be negligible up to degree $l = 100$ (Dombard & Sessa 2019).

Apart from the parameters of the seafloor power spectrum, we also vary the (a) radius of the seafloor or mantle, (b) spacecraft altitude, (c) compensation state of the seafloor, and (d) gypsum coverage on the seafloor. Computations of (a) and (b) are relatively simple, obtained by varying $\Delta\rho$ and z in Equation (3), where z is increased by the altitude of the spacecraft and $\Delta\rho$ is adjusted such that the mass of the silicate

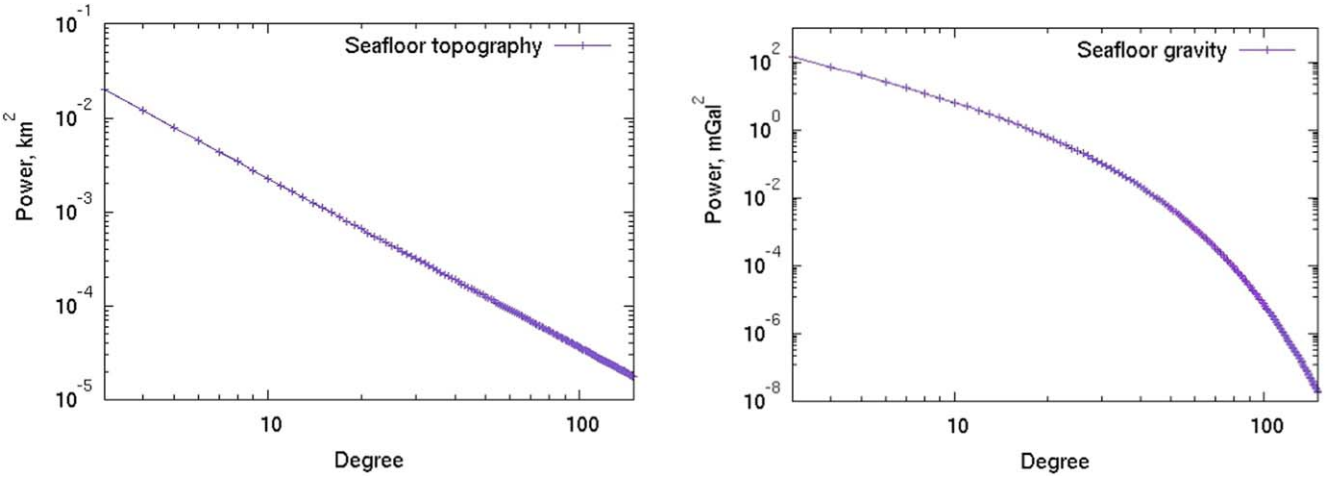

(a) Topography power spectrum (b) Gravity power spectrum

Figure 2. (a) Power spectrum of the seafloor topography, observed at an amplitude of 2 km and with a spectral slope β of -1.8. (b) Corresponding power spectrum of gravity obtained via Equation (3). The gravity signal of the mantle is reduced at higher degrees/shorter wavelengths owing to upward attenuation.

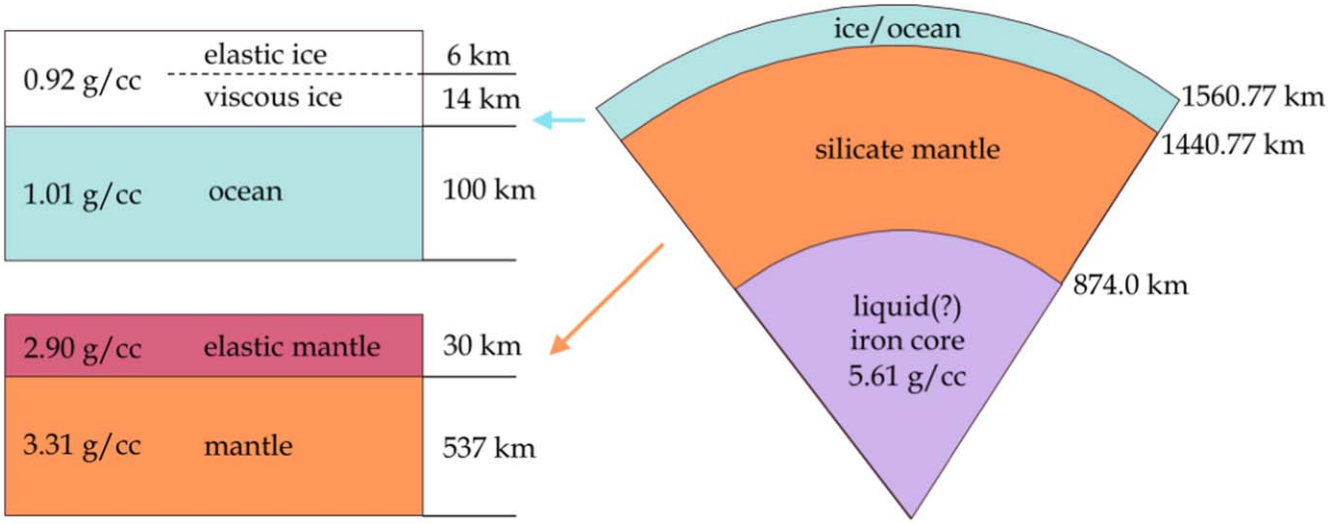

Figure 3. The assumed baseline interior structure of Europa. The thickness and densities of the H_2O layer and core are held constant as seen above, while the thickness and density of the silicate mantle layer (as well as its silicate crust) are varied. We use 0.92 g cc^{-1} for the density of ice (Tufts 1998) and 1.01 g cc^{-1} for the ocean, assuming pure water (Billings & Kattenhorn 2005). The normalized moment of inertia value for this structure is 0.354.

mantle stays constant. The purpose of this is to keep the bulk density of Europa, which is quite well determined to be 3.013 g cc^{-1}, constant while varying the thickness and density of the mantle as in Figure 3.

To account for (c) the effect of compensation at the seafloor, we follow the approach of Pauer et al. (2010) and Nimmo et al. (2011). At short wavelengths, loads are flexurally supported and hence uncompensated. At long wavelengths, loads cause the lithosphere to deflect, hence reducing topographic amplitude (Airy compensation). We account for this effect by multiplying each topographic coefficient by a factor F_l, the ratio of the resulting topography to the initial load at degree l, where

$$F_l = \frac{1}{1 + \frac{\rho_c - \rho_w}{\rho_m - \rho_c} C_l}. \quad (4)$$

In this equation ρ_c is the density of the crust, ρ_w is the density of the ocean, ρ_m is the density of the mantle, and C_l is defined as in Turcotte et al. (1981, Equation (27)), a quantity characterizing the degree of compensation. C_l is dependent on the degree l, the densities of the crust and mantle, and the rigidity of the lithosphere. Here the terms "crust" and "mantle" do not refer to the ice shell and silicate mantle, respectively, but rather a chemical distinction within the silicate layer where the "crust" is a lower-density (possibly hydrated) layer on the top and the "mantle" is the underlying higher-density silicate. We approximate ρ_c to be 2.9 g cc^{-1}, approximate ρ_m to be 3.31 g cc^{-1}, and assume a Poisson's ratio of 0.25, Young's modulus of silicate $E = 70$ GPa, and mean gravitational acceleration of $g = 1.3\,\mathrm{m\,s^{-2}}$. We then vary the elastic thickness, i.e., the thickness of the rigid part of the silicate crust, to consider different compensation states. We assume in this case that the elastic layer and crust have the same thickness, such that the mechanical and compositional layers of the mantle agree with one another.

We are interested in exploring (d) the coverage of gypsum owing to predictions by Melwani Daswani et al. (2021) that postulate a 3–10 km layer of gypsum sediment forming on

Europa's seafloor. We consider two end-member approaches to this problem. First, we explore a "uniform seafloor" approach, which treats gypsum sediment as flattening the silicate topography of the seafloor, such that the bottom of the ocean is a flat layer of gypsum. This results in no gravity signature from the gypsum–water interface due to the lack of topography, as well as a reduced gravity signature from the rock–gypsum interface due to the reduced density contrast (Equation (3)). In this case the thickness of the gypsum layer does not form an important factor apart from the assumption that it is sufficiently thick to exceed the peak topography of the seafloor.

Second, we consider the less likely possibility that the gypsum sediment acts as a "uniform blanket" that simply increases the height of the preexisting silicate topography by the thickness of the blanket. We consider this possibility less probable owing to the effect of ocean currents, which should serve to fill in topographic lows on the seafloor. In this case, we explore the predicted range of thicknesses 3–10 km, performing a rough approximation given that gypsum is $\approx\frac{1}{2}$ the density of silicate by increasing the size of the silicate layer by half the thickness of the gypsum blanket. This serves as a crude estimate to probe the effect of such a "uniform blanket" on the gravity signal of the seafloor, which should not be large. Note that these two approaches prescribe a generic treatment of a lower-density layer on Europa's seafloor, which could approximate both the gypsum precipitation described in Melwani Daswani et al. (2021) and the effects of possible serpentinization, though we acknowledge that the latter is potentially much thicker (Vance et al. 2018, Figure 9).

3. Model Results

Here we discuss the effect of varying specific aspects of our model (i.e., in the seafloor topography state or in the observation state, like during a flyby), while keeping all other aspects constant. The six parameters are (a) the amplitude of the seafloor topography's power spectrum, (b) its spectral slope, (c) the seafloor radius, (d) spacecraft altitude, (e) the compensation state of the seafloor, and (f) gypsum coverage on the seafloor. We discuss below the range explored for each parameter.

3.1. Baseline Scenario

Given each of the parameters above, our baseline estimate is that the amplitude and spectral slope of the power spectrum are approximately 2 km and −1.8, respectively. We also use a compensation state with an elastic thickness T_e of 30 km, a mantle radius of 1 440.77 km, and a spacecraft altitude of 50 km. With these parameters, the mantle gravity dominates up to spherical harmonic degree $l = 22$, after which the ice shell gravity becomes more detectable. This implies a spatial resolution of ≈410 km at the seafloor.

3.2. Topographic Amplitude

We choose a range of amplitudes to explore, from a small amplitude of 0.2 km to a large amplitude of 8 km (similar to lunar topography), keeping other parameters constant at the baseline value. Figures 4(a)–(f) show the longitude–latitude maps of the resulting seafloor gravity, as well as total gravity for the three cases. Figures 4(g)–(i) illustrate the total gravity at Europa Clipper's resolution of $l \approx 10$ (Mazarico et al. 2021) when the degree-2 tidal signal is excluded from the total signal. We also plot the power spectrum for the three cases (Figure 5), comparing the power of the seafloor's gravity signal with the gravitational power from our modeled ice shell topography (see the Appendix). A larger topographic amplitude for the seafloor would (self-evidently) correspond to a larger gravity contribution, so that at large amplitudes the seafloor topography becomes more noticeable than the ice shell in the total gravity signal.

To investigate the distinguishability of the seafloor topography from gravimetry, in this case and the following parameters we examine the intersection point in the power spectrum between seafloor gravity and ice shell gravity. This allows us to probe the degree up to which the seafloor forms the majority of the resulting total gravity signal. Here in the baseline scenario, where the field is measured at the surface, the seafloor gravity dominates up to harmonic degrees 5, 22, and 31, respectively, for the three amplitudes assumed. In the following subsections we vary parameters to explore the sensitivity of these results, and in Section 6 we discuss the implications.

3.3. Topographic Slope

We explore a range of spectral slopes centered about our best estimate, $\beta = -1.8$, keeping amplitude constant at 2 km. We also use slopes of −1.4 and −2.4, which are similar to the spectral slopes of Venus and Mars, respectively (Balmino 1993). Venus and Mars here act as terrestrial body analogs for the possible range of topographies of Europa's seafloor. A smaller spectral slope causes the mantle signal to dominate up to a higher degree, and vice versa (see Figure 6(a)). Here a Venus-like slope results in a crossover degree $l = 26$, while for a Mars-like slope the crossover occurs at $l = 15$.

3.4. Seafloor Radius

We explore a seafloor radius of 1440.77 and 1480.77 km, keeping the total mass of the silicate mantle and the bulk density of Europa constant (see Section 2). Here seafloor radius refers to the range of sizes of Europa's hydrosphere that we expect. A smaller mantle has a seafloor interface deeper within Europa, so its gravity signal is reduced by exponential upward attenuation. Hence, we find, as expected, that for a smaller mantle the mantle gravity contributes less to the total gravity, as shown in Figure 6(b). However, the effect is small (the crossover l changes by 4).

3.5. Spacecraft Altitude

We consider a range of spacecraft altitudes, from the gravity field at the surface to an altitude of 50 and 100 km above the surface. Notably, the current planned trajectory of Europa Clipper includes more than 40 flybys with observations of each latitudinal region at least as low as 50 km (some even lower at 25 km). At a higher altitude, the mantle signal undergoes more upward attenuation, but so does the ice shell's gravity signal (see Figure 6(c)). In general, we find that the wavelength at which the seafloor is detectable does not change much with spacecraft altitude owing to the upward attenuation of both these components.

3.6. Compensation State

Using the model described in Section 2, we consider the difference between a lithosphere that is uncompensated and a

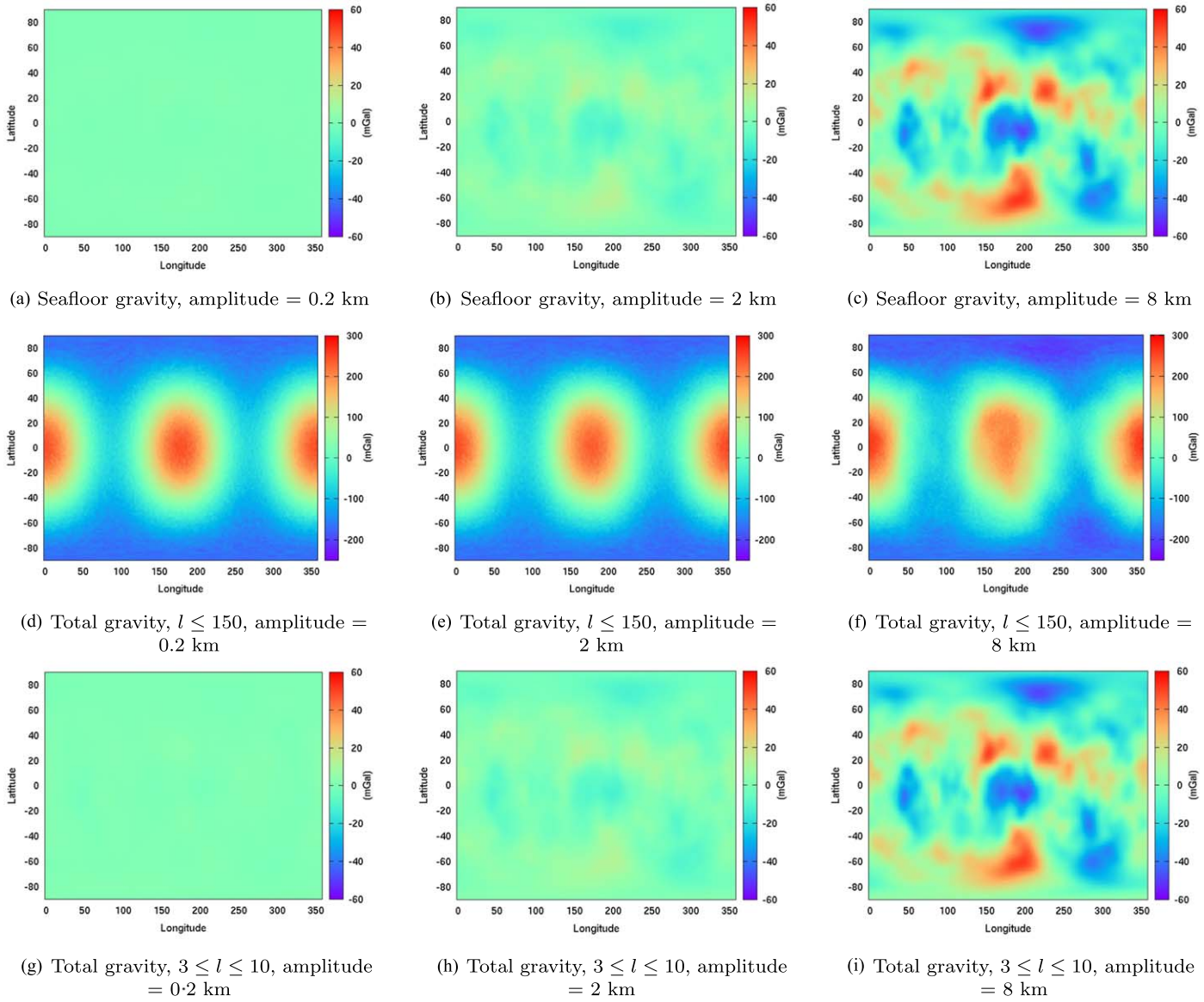

(a) Seafloor gravity, amplitude = 0.2 km (b) Seafloor gravity, amplitude = 2 km (c) Seafloor gravity, amplitude = 8 km

(d) Total gravity, $l \leq 150$, amplitude = 0.2 km (e) Total gravity, $l \leq 150$, amplitude = 2 km (f) Total gravity, $l \leq 150$, amplitude = 8 km

(g) Total gravity, $3 \leq l \leq 10$, amplitude = 0·2 km (h) Total gravity, $3 \leq l \leq 10$, amplitude = 2 km (i) Total gravity, $3 \leq l \leq 10$, amplitude = 8 km

Figure 4. Panels (a)–(c) show the seafloor topography given a spectral amplitude of 0.25, 2.5, and 10 km, respectively. Panels (d)–(f) show the corresponding total gravity signal. Panels (g)–(i) show the total gravity signal at the resolution of Europa Clipper, $l \approx 10$, when the degree-2 tidal signal is excluded.

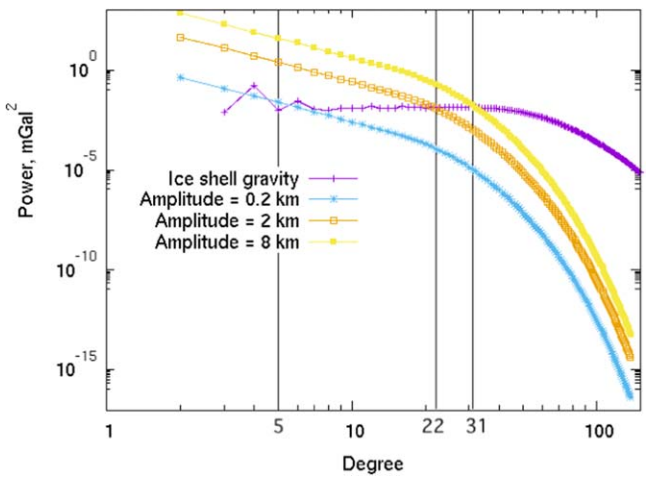

Figure 5. The power spectrum comparison of the seafloor's gravity signal vs. the ice shell gravity given the different amplitudes, plotted in log–log space.

compensated state with an elastic thickness T_e of 15 and 30 km, as shown in Figure 6(d). We expect that a body with a higher internal heat flux would have a thinner lithosphere and greater compensation. At longer wavelengths, loads are compensated more, leading to reduced power. Since $T_e = 15$ km corresponds to a high heat flux (Watts et al. 2013, Figure 4(c)), the range between this state and an uncompensated lithosphere spans the parameter space we would expect for the seafloor.

3.7. Layer of Gypsum

We consider the effect of a 3–10 km layer of gypsum sediment on the seafloor, using the two end-member approaches outlined in Section 2. For the uniform seafloor approach, wherein the seafloor is covered by a flat layer of gypsum that fills in the topography of the silicate mantle, we find that the gravity signal is reduced by the loss in density contrast at the rock–gypsum (originally rock–water)

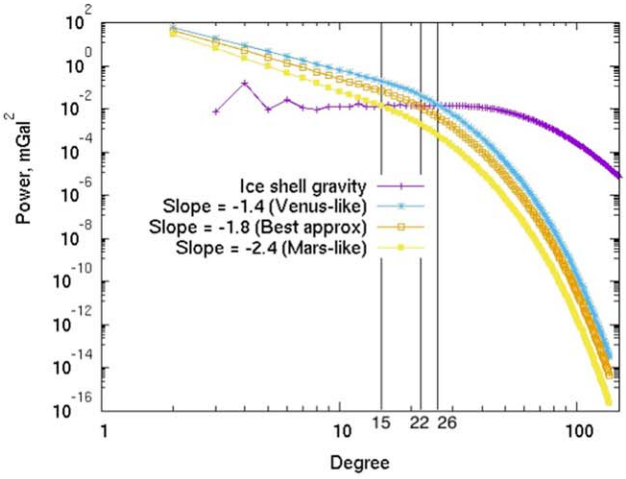

(a) Varying spectral slope

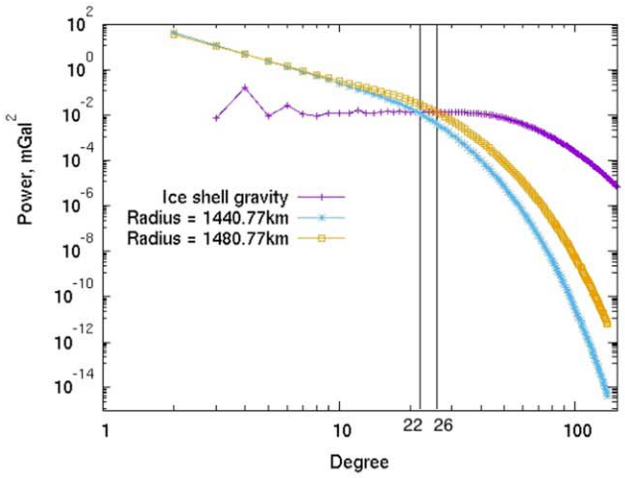

(b) Varying seafloor radius

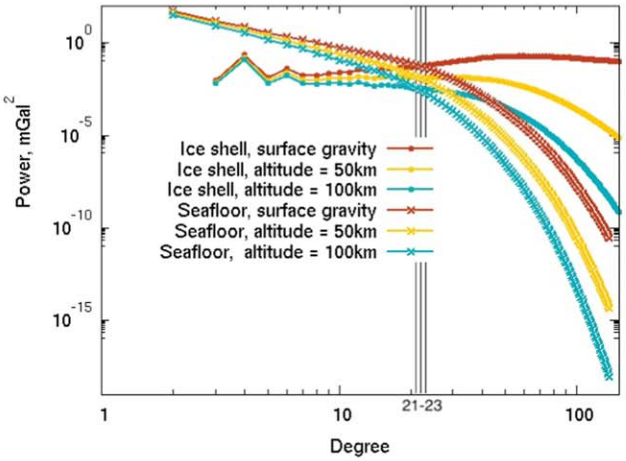

(c) Varying spacecraft altitude

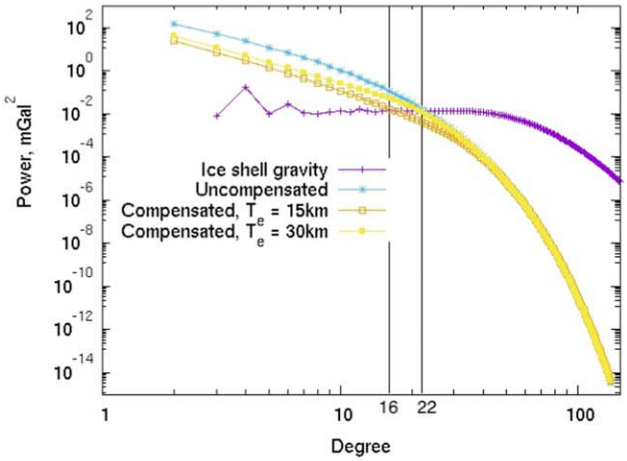

(d) Varying compensation state

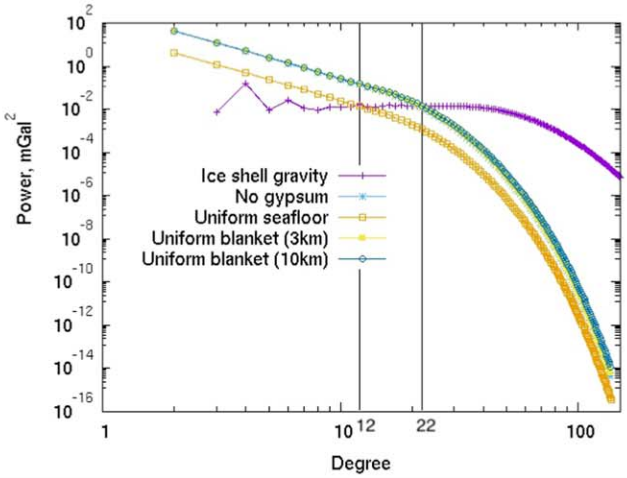

(e) Varying gypsum coverage

Figure 6. Panels (a)–(e) show the power spectrum comparison in log–log space of the seafloor's gravity vs. the ice shell gravity, if we vary different parameters. In panel (a) we vary the spectral slope of the seafloor topography, in panel (b) seafloor radius, in panel (c) spacecraft altitude, in panel (d) the compensation state of the seafloor, and in panel (e) the coverage of gypsum over the seafloor.

interface. The crossover degree is decreased significantly from $l = 22$ to $l = 12$. The uniform blanket approach, on the other hand, which instead presumes that the silicate topography is merely increased by the thickness of the gypsum layer, does not alter the gravity signal of the seafloor in any significant way.

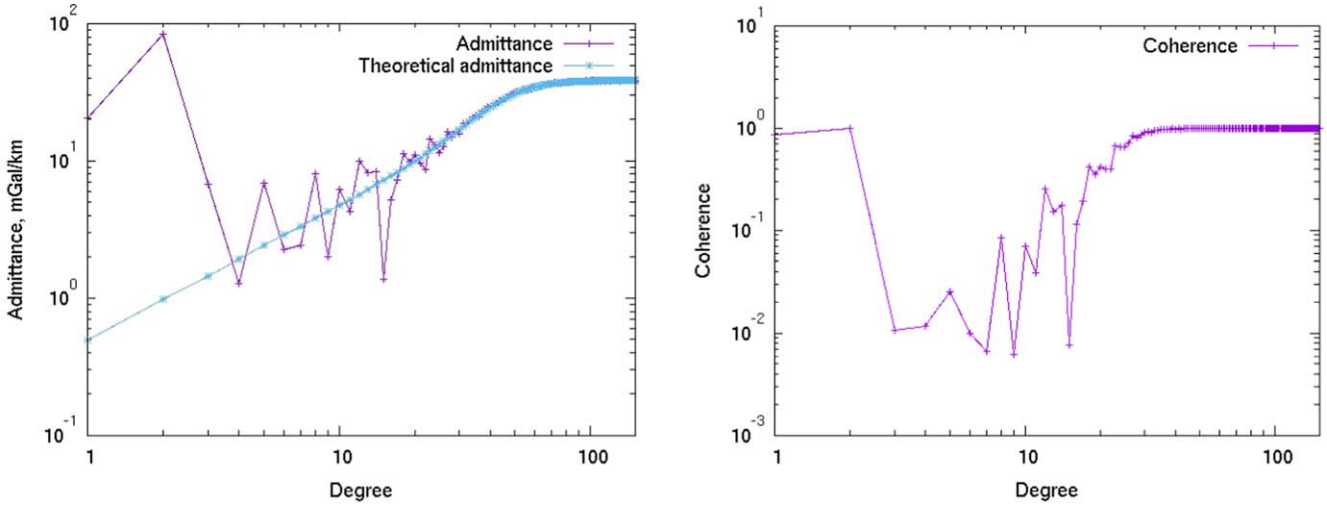

(a) Admittance (b) Coherence

Figure 7. Panels (a) and (b) show log–log plots of the admittance in mGal km^{-1} and coherence, respectively. In panel (a) we compare the admittance observed from our model to a theoretical value from Barnett et al. (2002).

4. Admittance and Coherence

In the interest of characterizing the relationship between surface gravity and surface (ice shell) topography, we also evaluate the admittance and coherence of our forward model (Akiba et al. 2022). We expect that at long wavelengths where the seafloor topography dominates the total gravity signal, surface gravity and topography are largely unrelated, whereas they should agree at short wavelengths where the seafloor signal has attenuated. If we express the load on the lithosphere as a Fourier series of loads at different wavelengths (Barnett et al. 2002), then the admittance is the ratio between the gravity anomaly caused by a load on the lithosphere and the magnitude of the topography. We can define admittance as Z(k) (from McKenzie & Fairhead 1997):

$$Z(k) = \frac{\langle \bar{g}\bar{h}^* \rangle}{\langle \bar{h}\bar{h}^* \rangle}. \quad (5)$$

Here k is the wavenumber, $\bar{g}$ and $\bar{h}$ are the Fourier transforms of the surface gravity and topography, respectively, the asterisks denote complex conjugates, and the angle brackets denote the average value over a wavenumber band centered at k. We should find at short wavelengths that, due to the linear correlation between surface gravity and surface topography, the admittance converges to a constant value:

$$Z = 2\pi\rho_u G, \quad (6)$$

where G is the gravitational constant and ρ_u is the density contrast of the surface load, which we can take to be the density of the ice shell 0.92 g cc^{-1}. Hence, the admittance is $Z \approx 40$ mGal km^{-1} at short wavelengths. Based on our computation of Equation (5), we observe that the admittance of our model behaves as we expect, converging to a constant value ≈40 mGal km^{-1} at short wavelengths (see Figure 7(a)). In this figure we compare our modeled admittance with the theoretical value we expect from Barnett et al. (2002), given by

$$Z(k) = \frac{3g_0(\rho_c - \rho_w)}{2a\rho_p} \exp(-kz) \times \left(1 - \exp(-kt_c)/\left(1 + \frac{ET_e^3k^4}{12(1-\sigma^2)(\rho_m - \rho_c)g_0}\right)\right), \quad (7)$$

where g_0 is the surface gravitational acceleration (1.314 m s^{-2}), ρ_c is the crustal density (0.92 g cc^{-1}), ρ_w is the density of its overlying fluid (0 g cc^{-1} for the vacuum), ρ_m is the "mantle" density (1.01 g cc^{-1} for the ocean), ρ_p is the mean density of Europa (3 g cc^{-1}), E is Young's modulus (9 GPa), T_e is the elastic thickness 6 km, σ is Poisson's ratio (0.3252), z is the spacecraft altitude (taken to be 0 km for our evaluation at the surface), and t_c is the mean "crustal" thickness (20 km). We conclude that the results of our model agree with this theoretical value at short wavelengths; Figure 6(a) shows that the admittance starts to become reliable at $l \approx 25$.

Additionally, we compute the coherence γ^2 between gravity and topography of our model, which is the ratio of cross-power spectra to auto-power spectra (McKenzie & Fairhead 1997):

$$\gamma^2 = \frac{\langle \bar{g}\bar{h}^* \rangle^2}{\langle \bar{g}\bar{g}^* \rangle \langle \bar{h}\bar{h}^* \rangle}. \quad (8)$$

We expect similarly that the surface topography and surface gravity should be completely coherent at short wavelengths where the ice shell dominates the gravity signal, causing the ratio to converge to 1. Our model results follow this expectation: at large wavelengths the gravity and topography are incoherent owing to the effect of the seafloor, but at short wavelengths ($l > 50$) the coherence converges to 1 (see Figure 7(b)).

5. Terrestrial Body Analogs

Apart from our general model approach, we also use other terrestrial bodies in the solar system as analogs for the possible states of Europa's seafloor. These bodies share similarities that

make them suitable parallels for Europa, for example, their silicate compositions and adherence to Kaula's law. We are primarily interested in the various forms a geologically active Europa could embody and hence focus on geologically active bodies like Earth, Venus, and Io. Tidal heating on Europa could cause high heat flows upward of 100 mW m^{-2} (Greenberg et al. 2002), which would certainly allow the possibility of a hot Europan mantle.

We choose Earth as a candidate owing to its unique plate tectonics, characterized by mid-ocean ridges, subduction zones, and fault lines. We also choose Venus and Io as hotter bodies with less efficient mantle convection mechanics, which both exhibit extensive volcanism, rejuvenated surfaces, and basaltic flows. Venus's surface, for example, features shield volcanoes and coronae, whereas Io serves as an interesting parallel owing to its similar size to Europa, although its increased tidal heating makes it a more extreme end-member in terms of geological activity.

We obtain surface topography data for Venus from the Magellan probe's altimetry analysis (Rappaport et al. 1999), as well as surface gravity data for Earth from the GRACE mission (Ries et al. 2016). There does not currently exist a global topographic or gravity map for Io; hence, we use topographic power estimates derived from limb profile analysis (White et al. 2014) to characterize Io's short-wavelength topography. We do this by randomly generating a set of spherical harmonic coefficients at each degree and constraining them to obey the estimated power. Note that in Ross et al. (1990) the derivation of long-wavelength topography assumes the surface topography of Io to be compensated at a fairly shallow depth, which would imply that the effective gravity signal at small degrees is small enough to be negligible.

Previous analyses exploring the gravity arising from Europa's seafloor assumed that seafloor topography is supported by a combination of lithospheric strength and Airy isostasy (Pauer et al. 2010; Dombard & Sessa 2019). Here, in order to scale the topographies of these terrestrial bodies, we expand the explored physics to consider topographic support arising from dynamic topography, i.e., supported by convection (Guimond et al. 2022). Such convection involves rising hot plumes, which flatten beneath the lid (lithosphere). The buoyancy gives rise to an upward stress, which results in surface topography h:

$$h \approx \alpha \Delta T \delta, \tag{9}$$

where α is the volumetric thermal expansivity, ΔT is the temperature contrast relative to the background material, and δ is the thickness of the hot region. In temperature-dependent convection, a thick "stagnant" lid develops, across which most of the temperature contrast occurs. The convecting region beneath the stagnant lid is characterized by temperature contrasts such that (Solomatov 1995)

$$\Delta T \approx \frac{R_g T_b^2}{Q}. \tag{10}$$

Here Q is the activation energy, R_g is the gas constant, and T_b is the basal temperature. For silicates we expect that $\Delta T \approx 50$–100 K. For a rising plume the maximum thickness of the hot region is the mantle thickness d. So the maximum dynamic topography we would expect from Equation (9) is $\alpha \Delta T d$. Taking $\alpha = 3 \times 10^{-5}$ K^{-1}, we expect a maximum dynamic topography of 4.5–9 km, which is a reasonable estimate of (for example) the long-wavelength dynamic topography of Venus (McKenzie 1994).

The resulting gravity anomaly Δg will be due to the surface topography (mass excess) and subsurface buoyant region (mass deficit). The latter will be attenuated by a factor e^{-kz}, where k is the wavenumber and z the depth. Integrating over the full vertical extent of the hot region assuming a Cartesian geometry, we find that for the subsurface region

$$\Delta g_{\rm sub} \approx -\frac{2\pi G \Delta \rho \alpha \Delta T}{k}(1 - e^{-kd}), \tag{11}$$

which reduces to the standard Bouguer (flat sheet) approximation in the limit of small kd. Here G is the gravitational constant and $\Delta \rho$ is the density contrast. If we further assert that the characteristic wavenumber of convection is controlled by the thickness of the convecting layer and thus scales as $1/d$, we see that

$$\Delta g_{\rm sub} \approx -2\pi G \Delta \rho \alpha \Delta T d(1 - e^{-1}). \tag{12}$$

Since the surface contribution is $\Delta g = +2\ \pi G \rho h$, the net gravity is

$$\Delta g \approx 2\pi G \Delta \rho h e^{-1}. \tag{13}$$

Note that e is Euler's number. For Venus, our estimate of Δg is approximately 200–400 mGal, which is very similar to observed results from Magellan (McKenzie 1994). This equation also gives us an admittance ($\Delta g/h \approx 45$ mGal km^{-1}) essentially identical to what is observed at convective rises on Venus (McKenzie 1994). Making use of Equation (9) and setting the thickness of the hot region to d, Equation (13) can be rewritten:

$$\Delta g \approx 2\pi G \Delta \rho \alpha \Delta T e^{-1} d, \tag{14}$$

which shows that the surface gravity resulting from dynamic topography should simply scale with the density contrast at the interface $\Delta \rho$ and the thickness of the mantle d, or (roughly speaking) the radius of the planet. For Europa's seafloor, which occurs at the ocean–mantle interface underneath the surface, we expect an additional attenuation term as in Equation (3).

We implement this scaling by computing the resultant gravitational anomaly if the surface topographies of these bodies were mapped onto Europa's seafloor. We do this by first scaling the surface topography by the size of the body (for the case of Europa, the size of its mantle). We then compute the resulting gravity of that topography if it were at Europa's ocean–mantle interface, i.e., using Equation (3) but substituting for Europa's seafloor's parameters. This effectively scales the resulting gravity by the density contrast at the interface, as well as upward attenuation to where the gravity is calculated. For Earth, where we have the set of gravity coefficients instead of surface topography, we scaled the gravity anomaly by the equivalent factor:

$$\Delta g \propto R_0 \Delta \rho \left(1 - \frac{z}{R}\right)^{l+2}, \tag{15}$$

where R_0 is the radius of the terrestrial body and the other variables are defined as in Equation (3).

This approach results in gravity spectra (see Figure 8) and shows that an Earth-like seafloor with plate tectonics would not be visible at short wavelengths beyond degree $l = 11$, whereas a Venus- or Io-like seafloor would dominate the gravity

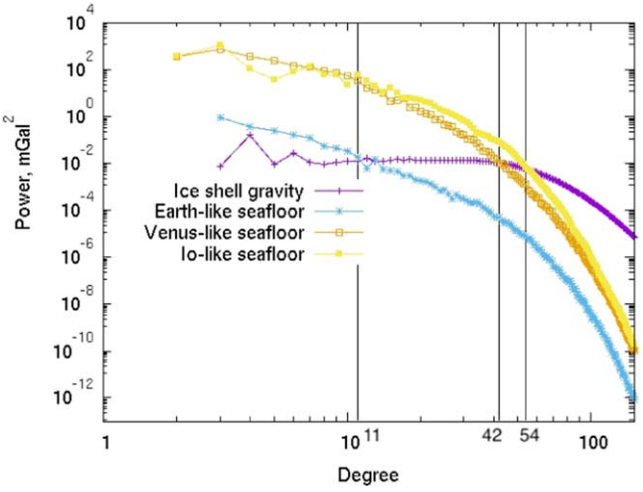

Figure 8. A power spectrum comparison of the ice shell gravity against the seafloor gravity, modeled using terrestrial bodes in the solar system as analogs, i.e., Earth, Venus, and Io.

spectrum up to degree $l = 42$ and 54, respectively. This implies a spatial resolution of ≈820 km for a (scaled) Earth-like seafloor, as well as ≈215 km for a (scaled) Venus-like seafloor and ≈170 km for an Io-like seafloor.

Given this, we might be able to detect a large Earth-like plate tectonic feature in the gravity signal of Europa if it were of order 820 km. For example, the largest mid-ocean rises on Earth would be visible at a resolution of degree 10, like the Mid-Atlantic Rise, which is ≈16,000 km long and 1000–1500 km wide. We would also be able to detect the signature of volcanically dominated geology, whether Venusian or Ionian in style. This is promising for our chances of characterizing a geologically active seafloor on Europa, given the likely gravity observations.

6. Discussion

Our results summarized in Sections 4 and 5 suggest considerable diagnostic capability for characterizing seafloor topography on Europa despite the intervening ocean and the contribution to the gravity of the topography of the overlying ice crust. However, this conclusion depends, as expected, rather sensitively on the amplitude of the anomalies. For the Earth-scaled case, the result is marginal; comparing the appearance of the terrestrial seafloor to the topography of Venus or Io at degree ≈10 leads to rather subtle differences that would be difficult to interpret in terms of terrestrial plate tectonics. However, the weakness of the seafloor gravity signal would itself convey some information: that the silicate mantle has a large degree of compensation, from which one might infer that the silicate part of Europa has a very thin lithosphere.

For the higher-amplitude gravity signatures such as would be appropriate for a Venus- or Io-like seafloor, the dominance out to degree 42 and 54, respectively, provides much better diagnosticity for interpreting the gravity in terms of a specific style of tectonics, volcanism, or, as in Dombard & Sessa (2019), a quiescent but heavily cratered topography.

Deposition of a 3–10 km thick blanket of gypsum can modestly reduce the signal, but probably not to the level where the high-amplitude gravity signature from the Venus- or Io-like topography would be completely obscured. It would, however, make it difficult to say something quantitative based on the amplitude of the gravity signature—to what extent the amplitude has been depressed by a gypsum layer.

Probing the ice shell with admittance techniques might be challenging. In all cases we examined, the ice shell signal does not dominate within the $l \approx 10$ resolution of the expected global gravity field. An alternative would be to use the observed line-of-sight acceleration to interpret local ice shell properties (James 2016; Roberts et al. 2018). Europa Clipper will probe the gravitational anomalies of the ice shell at the shortest wavelengths its sensitivity allows, particularly during its closest flybys to Europa's surface (Mazarico et al. 2021).

Finally, we emphasize the nonuniqueness of interpretation of the gravity field in terms of tectonic styles. We have considered several contrasting geologies, but as noted in Dombard & Sessa (2019), any number of mass distributions could produce a given gravity field. Interpretation will be illuminated by comparison with other bodies, but the history of unveiling new bodies—including the seafloor of the ocean world Europa—is replete with unexpected complications and surprises.

7. Conclusion

Power spectrum analysis of the gravity signal generated at Europa's seafloor, coupled with the estimated resolution of Europa Clipper's gravity experiment (Mazarico et al. 2021), indicates that the seafloor topography is detectable from a flyby gravity science experiment to a high enough degree and order such that the coarse style of Europa's mantle geology can be inferred. In the baseline scenario for the parameter space explored in this work, seafloor gravity dominates Europa's total gravity signal up to $l = 22$, while for planetary analogs we find that this occurs up to degree $l = 11$ for an Earth-like seafloor, as well as $l = 42$ and $l = 54$ for a Venus- and Io-like seafloor, respectively. The results for these analogs lead us to conclude that topographies related to plate tectonics and active volcanism can likely be distinguished on Europa's seafloor. Additionally, we find that a putative layer of gypsum (Melwani Daswani et al. 2021) may modestly reduce the strength of the gravitational signal of the seafloor by blanketing and flattening out the topography. However, we are unable to distinguish whether a given signal strength is affected by the gypsum layer, as we have no independent determination of topographic amplitude.

This work was supported by NASA through the Europa Clipper Project. Parts of this work were supported by J.P.L. award 1656356 and JHU-APL award 131512 (to F.N.) and J.P.L. award 1656436 (to J.L.).

Appendix

In the main text, we focus on the effect on the observable gravity of the mantle while holding the other gravity components constant. In this appendix we describe how these other components are derived.

(1) *Degree-2 coefficients:* The nonnormalized coefficients J_2 and C_{22} are set to 436×10^{-6} and 131×10^{-6}, respectively. This follows the Anderson et al. (1998) numbers, though recent numbers (e.g., Gomez Casajus et al. 2021) differ at the ≈5% level. Other degree-two coefficients are set to zero.

(2) *Long-wavelength shape:* Because of lateral variations in tidal heating, the shell thickness of Europa is expected to vary laterally (Nimmo et al. 2007). However, since the shell is

expected to be compensated at these wavelengths, the net effect on the gravity is small (peak-to-peak variation 3.4 mGal), even though the topography can be substantial. We use the specific shell thickness variation shown in Figure 4(a) of Nimmo et al. (2007) as our example.

(3) *Short-wavelength shape:* Finally, we assume a power-law topography for the ice shell at degree 3 and higher. Based on Nimmo et al. (2011, Figure 5), we take the power-law slope to be -1 and assume a peak-to-peak topography variation of 2 km. We assume that the topography is supported by an elastic layer, so that long-wavelength gravity anomalies are reduced owing to compensation. The resulting peak-to-peak gravity variation is 51 mGal but occurs primarily at short wavelengths because long wavelengths are compensated.

The shell thickness is taken to be 20 km and the elastic thickness to be 6 km. The gravity anomaly Δg_l at spherical harmonic degree l is given by

$$\Delta g_l = 4\pi G\rho h_l \frac{l+1}{2l+1}\left(1-\frac{d}{R}\right)^{l+2} C_l. \quad \text{(A1)}$$

Here G is the gravitational constant, ρ the surface density, h_l the topography at that degree, d the mean ice shell thickness, R the radius, and C_l the compensation factor. For an uncompensated short-wavelength feature, $\Delta g_l \rightarrow 2\pi G\rho h_l$ as expected. Compensation reduces the gravity anomaly, more so for a smaller elastic thickness (lower C_l) or a thinner ice shell. The quantity C_l is calculated using the expressions of Turcotte et al. (1981) taking the Young's modulus to be 9 GPa, Poisson's ratio 0.25, and ice shell and water densities of 0.92 and 1.01 g cc^{-1}, respectively.

ORCID iDs

Ze-Wen Koh https://orcid.org/0009-0006-0088-6667
Francis Nimmo https://orcid.org/0000-0003-3573-5915
Jonathan I. Lunine https://orcid.org/0000-0003-2279-4131
Erwan Mazarico https://orcid.org/0000-0003-3456-427X
Andrew J. Dombard https://orcid.org/0000-0001-7897-6079

References

Akiba, R., Ermakov, A. I., & Militzer, B. 2022, PSJ, 3, 53
Anderson, J. D., Schubert, G., Jacobson, R. A., et al. 1998, Sci, 281, 2019
Balmino, G. 1993, GeoRL, 20, 1063
Barnett, D. N., Nimmo, F., & McKenzie, D. 2002, JGRE, 107, 5007
Billings, S. E., & Kattenhorn, S. A. 2005, Icar, 177, 397
Dombard, A. J., & Sessa, A. M. 2019, Icar, 325, 31
Gomez Casajus, L., Zannoni, M., Modenini, D., et al. 2021, Icar, 358, 114187
Greenberg, R., Geissler, P., Hoppa, G., & Tufts, B. R. 2002, RvGeo, 40, 1004
Guimond, C. M., Rudge, J., & Shorttle, O. 2022, PSJ, 3, 66
James, P. B. 2016, LPSC, 47, 2513
Jeffreys, H. 1976, The earth. Its origin, history and physical constitution. (6th ed.; Cambridge: Cambridge Univ. Press)
Mazarico, E., Buccino, D. R., Castillo-Rogez, J., et al. 2021, LPSC, 52, 1784
McKenzie, D. 1994, Icar, 112, 55
McKenzie, D., & Fairhead, D. 1997, JGR, 102, 27,523
Melwani Daswani, M., Vance, S. D., Mayne, M. J., & Glein, C. R. 2021, GeoRL, 48, e94143
Nimmo, F., Bills, B. G., & Thomas, P. C. 2011, JGRE, 116, E11001
Nimmo, F., Thomas, P., Pappalardo, R., & Moore, W. 2007, Icar, 191, 183
Pauer, M., Musiol, S., & Breuer, D. 2010, JGRE, 115, E12005
Phillips, R., & Wieczorek, M. 1998, JGR, 103, 1715
Rappaport, N. J., Konopliv, A. S., Kucinskas, A. B., & Ford, P. G. 1999, Icar, 139, 19
Ries, J., Eanes, R., Kang, Z., et al. 2016, The Development And Evaluation of The Global Gravity Model, CSR-16-02 Univ. Texas at Austin, https://doi.org/10.26153/tsw/1461
Roberts, J. H., Vance, S., & Ganse, A. 2018, AGUFM, P42B–06
Ross, M. N., Schubert, G., Spohn, T., & Gaskell, R. W. 1990, Icar, 85, 309
Russell, M., Hall, A., & Martin, W. 2010, Geobiology, 8, 355
Schubert, G., Sohl, F., & Hussmann, H. 2009, in Europa, ed. R. T. Pappalardo, W. B. McKinnon, & K. K. Khurana (Tucson, AZ: Univ. Arizona Press), 353
Solomatov, V. S. 1995, PhFl, 7, 266
Tufts, B. R. 1998, PhD thesis, Univ. Arizona, http://hdl.handle.net/10150/282707
Turcotte, D. L., Willemann, R. J., Haxby, W. F., & Norberry, J. 1981, JGR, 86, 3951
Vance, S. D., Panning, M. P., Stähler, S., et al. 2018, JGRE, 123, 180
Verma, A. K., & Margot, J.-L. 2018, Icar, 314, 35
Watts, A., Zhong, S., & Hunter, J. 2013, AREPS, 41, 443
White, O. L., Schenk, P. M., Nimmo, F., & Hoogenboom, T. 2014, JGRE, 119, 1276